Apical Charge Flux-Modulated In-Plane Transport Properties of Cuprate Superconductors

Sooran Kim,[†] Xi Chen, William Fitzhugh, and Xin Li[*]

John A. Paulson School of Engineering and Applied Sciences, Harvard University, Cambridge, Massachusetts 02138, USA

For copper-based superconductors, the maximum superconducting transition temperature $T_{c,\max}$ of different families measured from experiment can vary from 38 K in La_2CuO_4 to 135 K in $HgBa_2Ca_2Cu_3O_8$ at the optimal hole doping concentration. We demonstrate herein, using *ab initio* computations, a new trend suggesting that the cuprates with stronger out-of-CuO_2-plane chemical bonding between the apical anion (O, Cl) and apical cation (e.g., La, Hg, Bi, Tl) are generally correlated with higher $T_{c,\max}$ in experiments. We then show the underlying fundamental phenomena of coupled apical charge flux and lattice dynamics when the apical oxygen oscillates vertically. This triggers the charge flux among the apical cation, apical anion, and the in-plane CuO_4 unit. The effect not only dynamically modulates the site energy of the hole at a given Cu site to control the in-plane charge transfer energy, but also can modulate the in-plane hole hopping integral simultaneously in a dynamic way by the cooperative apical charge fluxes.

Since the discovery of high-temperature superconductivity in hole-doped La_2CuO_4 [1], there has been a long-standing debate on the underlying mechanism. All the copper-based superconductors or cuprates have the common CuO_2 planes as the superconducting layers. They can be considered as being transformed from the Mott insulators by doping the CuO_2 planes. It was considered that strong electronic correlations and spin fluctuations in CuO_2 planes play some essential role here [2–4]. However, other phenomena like abnormal phonons or lattice effects, stripe or nematic charge orderings, spin glass phases, charge and spin density waves, and pseudogap state constantly add the complexity to the understanding of high-T_c superconductivity [5–13].

It has been noticed that simplifying the cuprates into the 2D square lattice rules out some essential physics behind all these complicated phenomena. For example, despite the same structural building block of CuO_2 layers, experimental $T_{c,\max}$ varies a lot among different families of cuprates. Some previous works were trying to integrate the out-of-plane factors into the mechanism. Ohta *et al.* suggested the Madelung potential of the apical oxygen as a material-dependent parameter controlling the stability of Zhang-Rice singlets and also T_c [14]. Pavarini *et al.*, using first principle calculations, reported that $T_{c,\max}$ increases with the apical oxygen height d_A and further calculated the hopping range parameter inside the CuO_2 plane [15]. The argument was that larger apical oxygen height weakens the interlayer hopping, while it strengthens the longer ranged intralayer hopping. In addition, the charge transfer energy between the in-plane Cu and oxygen, $\epsilon_d - \epsilon_p$, was introduced as a relevant parameter tuned by the apical

oxygen height [16]. Furthermore, the energy level offset between d_{x2-y2} and d_{z2} of the in-plane Cu, $E_{x2-y2} - E_{z2}$, was considered as a parameter for higher T_c by minimizing the Cu $3d_{z2}$ character of the Fermi surface [17–19].

Although the previous works tend to explain higher T_c in cuprates by the out-of-plane static modulation for stronger 2D behavior of CuO_2 planes, the recent report of light-induced superconductinglike behavior in $YBa_2Cu_3O_{6+x}$ indicates that such explanation might be oversimplified. The apical oxygen distortions are selectively driven by the midinfrared optical pulse to give the resonant excitation of the apical oxygen phonon mode along the out-of-plane direction, which leads to the optically induced coherent transport up to room temperature (300 K) [20–22]. Despite the complicated underlying mechanism, the experiment at least suggests the importance of the apical lattice dynamics on modulating the in-plane transport properties, while the previous models mentioned above all focused on various *static* modulations.

In this Letter, we show by density-functional theory (DFT) simulations that the "apical structure unit," formed by the in-plane Cu and its nearest oxygen neighbors, the apical anion, and the apical cation along the c axis [inset in Fig. 1(a)], is a fundamental building block that can couple dynamically to control the superconductive properties. Specifically, we show that the bonding strength between the apical cation and apical anion is positively correlated with experimental $T_{c,\max}$ across the hole-doped cuprates. Underlying this new trend, we find that an apical dynamic charge transfer can be triggered effectively by the vertical ultrafast oscillation of apical ions. We further discuss how a process of cooperative apical charge fluxes (CACFs) can
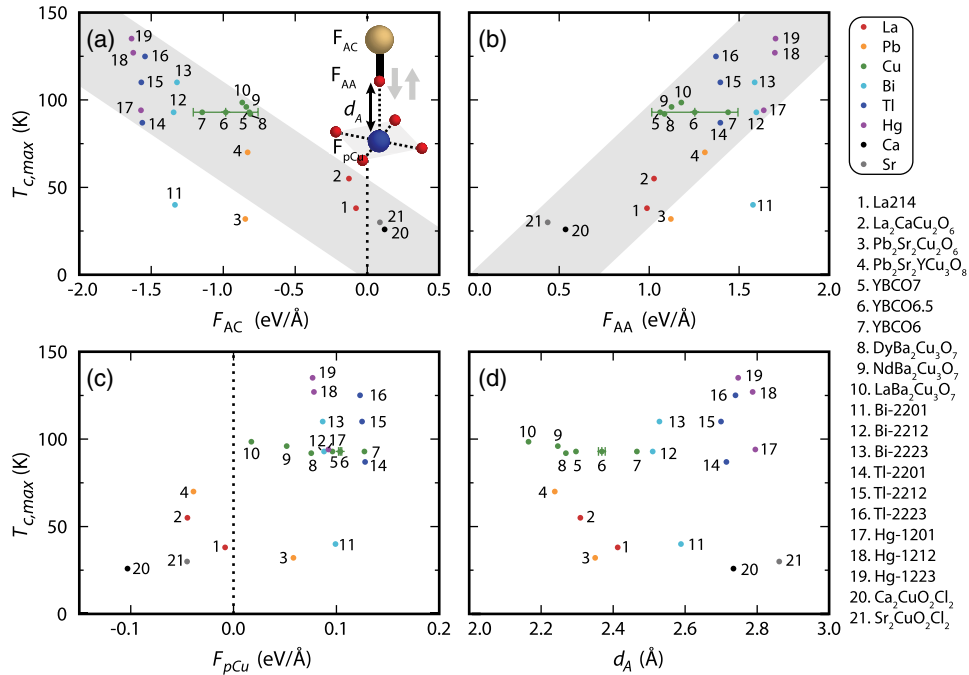
FIG. 1.   Apical forces by the apical anion distortion versus $T_{c,\max}$ for hole-doped cuprates. (a) Forces on the apical cation (F_{AC}), (b) forces on the apical anion (F_{AA}), and (c) forces on the planar Cu (F_{pCu}) with the apical anion distortion toward the CuO_2 plane. (d) $T_{c,\max}$ versus apical anion height d_A. Colors represent the type of apcial cation of each family. Error bars indicate the apical Cu in empty and filled CuO chains along the b axis of YBCO6.5. The inset in (a) represents the structure unit formed by a planar Cu, its nearest four oxygen neighbors, an apical anion, and an apical cation along the c axis. The apical forces on the apical cation, anion, and planar Cu, caused by vertical distortion of the apical anion, are labeled as F_{AC}, F_{AA}, and F_{pCu}, respectively.

effectively modulate the in-plane transport property by dynamically changing both charge transfer energy and hopping integral. The model here distinguishes from the previous models by explicitly introducing several coupled ultrafast dynamic processes as fundamental building blocks for the charge transport mechanism in cuprates, which connects well with several new ultrafast and photoemission experiments that show the importance of such dynamic processes [5,6,20–22].

All DFT calculations were performed by the Vienna *ab initio* simulation package (VASP) [23]. The projector augmented wave Perdew-Burke-Ernzerhof functional was utilized for the exchange-correlation energy. PHONOPY was employed for phonon calculations [24]. For force, density of states (DOS), and phonon calculations, we have performed the nonspin polarized DFT $+ U$ calculations with $U = 8$ eV and $J = 1.34$ eV for the correlated d orbitals of Cu [25]. The force and DOS calculations are also checked by hybrid functional HSE06. Polaron calculations were performed using HSE06 and the G-type antiferromagnetic ordering in CuO_2 layers as an initial magnetic configuration [26]. Computational method details are in the Supplemental Material [27].

To quantify the bond strength between the apical cation and apical anion, we calculate the apical forces by manually distorting the apical anion along the directions shown by the

arrows in the inset of Fig. 1(a). The forces with the apical anion moving 0.12 Å toward the CuO_2 plane are shown in Figs. 1(a)–(c), while the forces by apical anion moving 0.12 Å away from the plane are shown in Fig. S1 [27]. $T_{c,\max}$, d_A and abbreviations of materials are summarized in Table S1 [27].

First, the family with higher experimental $T_{c,\max}$ in general shows larger magnitude of F_{AC} in Fig. 1(a) and F_{AA} in Fig. 1(b) for hole-doped cuprates, suggesting that the bonding between the apical cation (AC) and apical anion (AA) is a descriptor strongly correlated with high T_c superconductivity. Second, the materials in the same family (same color) show a similar magnitude of apical forces regardless of the number of CuO_2 layers, suggesting the fundamental materials-dependent role of the apical force. Third, the chemical bond between the apical cation and apical anion is different from the bond between the apical anion and planar Cu. F_{pCu} in Fig. 1(c) shows less obvious correlation with $T_{c,\max}$ and almost 10 times smaller magnitude than F_{AC} and F_{AA}. Hence, the frequencies of the apical anion oscillations are majorly controlled by the bonding to the apical cation. Fourth, the oxygen vacancies in YBCO6.5 and YBCO6 only slightly change the apical force without disturbing the general trend in Figs. 1(a) and 1(b). The force of YBCOX ($X = 6$, 6.5, and 7) is larger than that of the La family and smaller than that in the Hg

family. It suggests that the trend is majorly about the materials dependence of $T_{c,\text{max}}$ rather than the doping dependence of T_c. Further details are in the Supplemental Material [27].

This correlation highlights the role of the bond strength between the apical anion and the apical cation, which can directly control the lattice dynamics or phonon of the apical anion. We also found the correlation between phonon frequency of apical oxygen along the c axis and $T_{c,\text{max}}$ (Fig. S3) [27]. These results are consistent with our force calculations and the previous Raman scattering experiments (Table S2) [27,61–66].

Figure 1(d) shows that the correlation of apical anion height d_A with $T_{c,\text{max}}$ is less obvious compared with the apical forces. We cannot simply compare d_A of the apical Cl materials (#20, #21) to that of apical O materials, while we can compare their apical forces, which follow the trend in Figs. 1(a) and 1(b). Also note that because of the in-plane Cu buckling d_A of $R\text{Ba}_2\text{Cu}_3\text{O}_7$ ($R =$ Y, La, Nd, and Dy) with $T_{c,\text{max}}$ of $\sim$100 K are smaller than d_A of the La family with $T_{c,\text{max}} \lesssim 55$ K. Therefore, the apical force is a more relevant and universal descriptor for cuprates than the apical anion height. More importantly, the apical chemical bonding naturally relates to the dynamic effects of coupled apical ion and charge oscillations.

Figure 2 shows the typical charge redistribution by the apical oxygen distortion in cuprates. When the apical oxygen moves toward the CuO_2 plane, the electron density on the apical cation increases and that on the planar orbitals decreases [Fig. 2(a)]. This suggests the out-of-plane electron flux by the inward oxygen movement. When the apical oxygen moves away from the CuO_2 plane, the charge flows oppositely. The partial DOS (PDOS) of the apical cation of Tl, the apical anion O, and the planar Cu exhibit consistent results [Fig. 2(b)]. When the apical oxygen is closer to the CuO_2 plane, the PDOS of the apical cation and oxygen lowers in energy, whereas that of the planar Cu and O increases in energy, corresponding to the charge transfer from the planar CuO_4 unit to the apical oxygen and cation. When the apical oxygen moves away from the CuO_2 plane, the PDOS of apical oxygen and cation shifts upward with a non-negligible portion of DOS moving above the Fermi level, forcing the electron to flow toward the plane.

Furthermore, similar to the apical force trend, the capability of the band structure to accommodate the dynamic apical charge flux is correlated with $T_{c,\text{max}}$. The hybridization of unoccupied bands from the apical cation and p orbital of the apical anion shows a general trend that, the closer the hybridization peak is to the Fermi level (E_f), the higher the $T_{c,\text{max}}$ is. For example, the dotted line in Fig. 2(b) shows the sharp hybridization peak of unoccupied DOS for Tl-2212 above E_f. The peak positions of three family groups of (Tl, Hg, Bi), (Y), and (Pb) are roughly 1, 2, and 3 eV above E_f, respectively, leading toward less effective apical charge transfer with decreasing
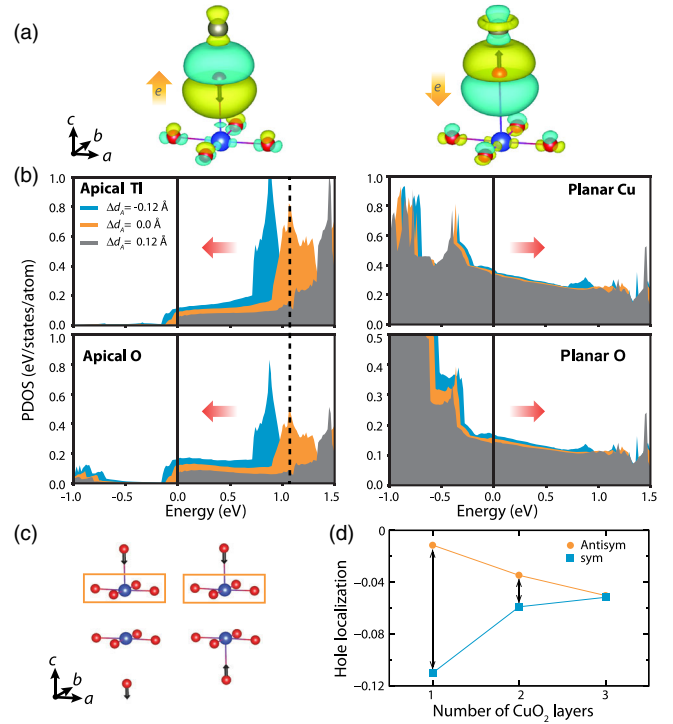
FIG. 2. Charge transfer with the apical oxygen distortion. (a) The electron density difference between the distorted structure and the equilibrium structure of Tl-2212. (Left) $\Delta d_A = -0.12$ Å. (Right) $\Delta d_A = 0.12$ Å. Yellow and green lobes represent the positive and negative parts, respectively. Gray and orange arrows indicate the direction of the apical oxygen distortion and the associated electron flux, respectively. (b) The PDOS of the apical cation of Tl, the apical oxygen, the planar Cu, and the planar O of Tl-2212. The dotted line marks the peak position for the hybridization of unoccupied bands between the apical Tl and apical O at around 1.1 eV above the Fermi level. (c) Antisymmetric (left) and symmetric (right) apical oxygen distortions. The distortion of each oxygen position is 0.12 Å. (d) Hole localization on the CuO_4 unit with antisymmetric (antisym) and symmetric (sym) apical oxygen distortions depending on the number of CuO_2 layers in Tl-2201, Tl-2212, and Tl-2223, respectively. The CuO_4 unit is indicated by the orange box in (c). The two oxygen ions are moved toward each other in the symmetric mode in (d).

$T_{c,\text{max}}$. The La family, $\text{Ca}_2\text{CuO}_2\text{Cl}_2$, and $\text{Sr}_2\text{CuO}_2\text{Cl}_2$ show even weaker hybridization because the empty bands of the apical cation are located at around 4–6 eV above E_f. Their apical cations just provide the electrons to the apical anion rather than forming the hybridization. The trend discussed in Fig. 2 is consistent with the hybrid functional calculation in Fig. S4 [27]. The Bader charge of apical oxygen decreases in Fig. S5 [27] from the La family toward the Hg family by 0.24 electrons, indicating increasing strength of covalent bonding between the apical cation and apical oxygen. Therefore, the stronger bonding and force between the apical cation and apical anion is caused by their stronger hybridization, which gives more effective apical charge transfer.

Even though the force trend in Fig. 1 does not show the layer dependence, its coupled dynamic effect through the dynamic charge transfer can be strongly influenced by the number of CuO_2 layers. Figure 2(c) shows the two representative modes of apical oxygen distortions with either antisymmetric or symmetric movements about the central CuO_2 layers. Hole localization in Fig. 2(d) is defined as the difference in Bader charges of the in-plane CuO_4 unit with and without apical oxygen distortions. The negative sign indicates the localized hole induced by the distortion. The charge transfer or hole localization on the in-plane CuO_4 unit shows the strongest influence by the mode of apical oxygen distortion in the single layer case, while such influence weakens with increasing number of CuO_2 layers due to a stronger interlayer screening effect. At the single layer, the symmetric mode shows much stronger hole localization than the antisymmetric mode, while such difference decreases at double layers and varnishes at triple layers. Since both oscillation modes can exist in cuprates, the dynamic hole localization and charge transfer can be perturbed at maximum at single layer due to the superposition of the two apical oxygen modes at a given Cu site. Furthermore, in Fig. 2(d), the difference of such perturbation effect between one layer and two layers is larger than that between two and three layers. The trend is also consistent

with the layer dependence of $T_{c,\max}$, where $\Delta T_{c,\max}$ between one and two layers is always larger than that between two and three layers. The charge density difference between the distorted and the equilibrium structures in Fig. S6 illustrates the hole localization, which is consistent with the Bader analysis [27].

We find that the apical phonon modes and the in-plane ones, such as the breathing modes, can couple in hole-doped cuprates (Fig. S7 [27]). When the apical oxygen moves toward the in-plane Cu, the surrounding in-plane oxygens also move toward the central Cu in such dynamic phonon couplings, and vice versa. Such coupling is consistent with the dynamic charge transfer characteristic of cuprates, as when the apical oxygen moves toward the plane, electrons flow outward away from the in-plane CuO_4 unit, driving the shrinkage of the in-plane Cu–O bond length. We also note that the frequency of apical oxygen phonon mode near 50–70 meV here coincides well with the "kink energy" from photoemission measurements [5,6], suggesting the possible coupling of such apical oxygen oscillations with the in-plane charge carrier motion.

Based on the above discussions in Fig. 2 and Fig. S7 [27], we introduce a new mechanism of coupled ionic and electronic oscillations to modulate the in-plane transport property. We demonstrate this new transport mechanism by
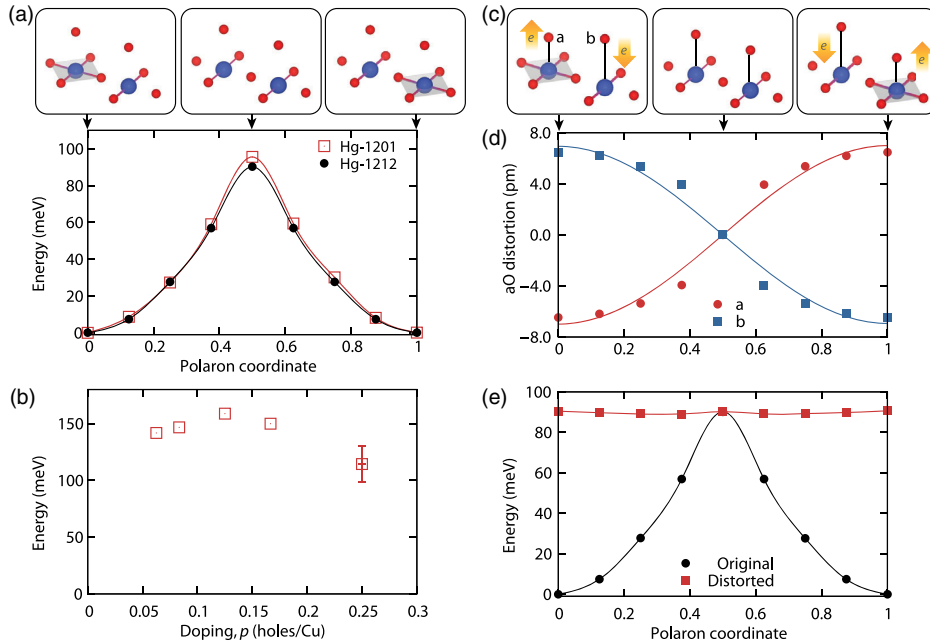
FIG. 3. Small polaron activation barrier without and with the apical oxygen modulation. (a) Comparison of the activation barrier between Hg-1201 and Hg-1212. The scheme on top shows how the small polaron migrates between neighboring Cu sites. The gray area indicates the polaron position. (b) Activation barrier depending on the hole doping level in Hg-1201. The error bar is from different sizes of supercells with the same hole doping concentration. (c) Cooperative distortions of the polaron migration and the apical oxygen distortion. The apical oxygen distortions are exaggerated for convenience in visualization. Two yellow arrows indicate the direction of CACFs. (d) Actual apical oxygen distortions added to the configuration $\{q_x\}$ on the polaron migration pathway. Data are fitted with a simple harmonic oscillator. (e) Reduced small polaron activation barrier of Hg-1212 with the apical oxygen distortions (red) compared with the original activation barrier (black).

the simulation of small polaron migration. More computational details on polaron simulations are in Fig. S8 [27]. Note that such mechanism is not limited to small polarons but can be applied to any forms of holes, including large polarons or quasiparticles. We choose a small polaron here as it is the least expensive DFT simulation to demonstrate such mechanism.

Figure 3(a) illustrates how the small polaron migrates between two neighboring Cu sites without the apical oxygen modulation. The calculated activation barriers of the hole polaron are 90 and 96 meV for Hg-1212 and Hg-1201, respectively, at a hole doping level of $p = 0.25$. Using different supercell sizes of the Hg-1201 structure, we explored the activation barrier at each hole concentration [Fig. 3(b)], which ranges from 114 meV at $p = 0.25$ to 160 meV at $p = 0.125$. These barriers will localize any such polaron hole in the temperature range of interest.

However, with the apical charge flux that can be generated by apical oxygen oscillation, the hopping barrier can be largely reduced. Ideally, if CACFs are associated with the opposite directions of apical oxygen oscillations in the neighboring Cu sites, the in-plane oxygen oscillations around the two Cu sites will also be coupled accordingly. Such CACF process is supported by the local charge neutrality condition of the apical charge-up in one Cu site, balanced by the apical charge-down in another neighboring Cu site. Figure 3(c) illustrates how this mechanism can modulate the small polaron migration barrier between the neighboring Cu sites.

The magnitude of such apical oxygen distortions at different coordinates on the polaron migration pathway is shown in Fig. 3(d) with the curve shape reminiscent of the typical phonon motions of a simple harmonic oscillator. The maximum amplitude of distortion here is around 6.5 pm/atom, which is reasonably small compared with the calculated apical phonon amplitude u of 8.4 pm at zero point energy using $u = \sqrt{2\hbar/M\omega}$, where M and ω are the oxygen mass and apical phonon frequency of 75 meV in this particular case, respectively. The set of relative apical oxygen distortions in Fig. 3(d) is then added to the set of cell configurations $\{q_x\}$ to calculate the modulated small polaron migration barrier. We find that such cooperative apical oxygen distortions significantly reduce the small polaron activation barrier to a small value of 1.6 meV as shown in Fig. 3(e). If the cooperative apical oxygen modulations follow exactly the simple harmonic path in Fig. 3(d), the polaron activation barrier is reduced to 34 meV instead.

It is worth noting that the above ideal situation of cooperative oscillation of the neighboring apical oxygens is not necessarily required to assist a single hopping case, because as long as the apical oxygen on top of the polaron Cu site is oscillated at a phase near the CuO_2 plane, but is moving away, the polaron site energy is increased and the hopping barrier is reduced, giving an asymmetric energy profile. However, at lowered temperature with reduced temperature fluctuation, the aforementioned CACF process at the neighboring apical oxygen sites [Figs. 3(c)–3(e)] can better help the continuous or even coherent in-plane charge flow.

From an energy perspective, the apical lattice vibration energy, which is proportional to its frequency and apical force, is effectively transferred locally by this dynamic mechanism to both strengthen the in-plane charge hopping integral [Fig. 3(e)] and instantaneously reduce the charge transfer energy by shifting the d_{x2-y2} orbital to a lower energy direction (Fig. S9 [27]). Notably, the phonon frequency of around 50–80 meV, depending on the family (Fig. S3 and Table S2 [27]), is comparable to the migration barrier of ~100 meV for small polaron, while the barrier is even smaller for holes with larger spatial ranges. The cuprates with higher apical phonon frequencies are associated with more robust apical charge flux, which can strengthen the in-plane charge hopping more effectively with less susceptibility to the temperature fluctuation.

We note that the previous descriptor of in-plane charge transfer energy [16] and hopping integral [15] can be integrated into our model in a dynamical way by coupling with the apical charge oscillation. Our proposed dynamic mechanism here can connect with several dynamic experimental phenomena that indicate the unconventional interplay between electron and phonon interactions [5,6,20–22]. Moreover, previous observation of T_c being influenced more by the chemical disorder near the apical oxygen than between CuO_2 layers [67] can be related to their stronger disturbance to the proposed CACF process. Interestingly, our model also provides a mechanism to mobilize the otherwise localized small polaron that possibly exists in the parent cuprates [68], although our model is not limited to small polaron.

In conclusion, we found the new trend that in hole-doped cuprates the family with higher $T_{c,\max}$ is correlated with stronger apical chemical bonding and hybridization. Based on this, we proposed a new dynamic mechanism of coupled CACFs and the lattice oscillations to modulate the in-plane charge hopping processes. We believe our understanding here can shed light on the understanding of the complicated phenomena in cuprates, especially how the transport properties are controlled by the coupled electronic and ionic dynamic oscillations.

*Corresponding author.
lixin@seas.harvard.edu
†Present address: Department of Physics Education, Kyungpook National University, Daegu, 41566, Korea.

[1] J. G. Bednorz and K. A. Müller, Z. Phys. B **64**, 189 (1986).

[2] P. A. Lee, N. Nagaosa, and X.-G. Wen, Rev. Mod. Phys. **78**, 17 (2006).

[3] N. Nagaosa and P. A. Lee, Phys. Rev. Lett. **64**, 2450 (1990).

[4] D. J. Scalapino, Rev. Mod. Phys. **84**, 1383 (2012).

[5] A. Lanzara, P. V. Bogdanov, X. J. Zhou, S. A. Kellar, D. L. Feng, E. D. Lu, T. Yoshida, H. Eisaki, A. Fujimori, K. Kishio, J.-I. Shimoyama, T. Noda, S. Uchida, Z. Hussain, and Z.-X. Shen, Nature (London) **412**, 510 (2001).

[6] Z.-X. Shen, A. Lanzara, S. Ishihara, and N. Nagaosa, Philos. Mag. B **82**, 1349 (2002).

[7] S. Ishihara and N. Nagaosa, Phys. Rev. B **69**, 144520 (2004).

[8] S. A. Kivelson, I. P. Bindloss, E. Fradkin, V. Oganesyan, J. M. Tranquada, A. Kapitulnik, and C. Howald, Rev. Mod. Phys. **75**, 1201 (2003).

[9] F. C. Chou, N. R. Belk, M. A. Kastner, R. J. Birgeneau, and A. Aharony, Phys. Rev. Lett. **75**, 2204 (1995).

[10] J. M. Tranquada, B. J. Sternlieb, J. D. Axe, Y. Nakamura, and S. Uchida, Nature (London) **375**, 561 (1995).

[11] W. D. Wise, M. C. Boyer, K. Chatterjee, T. Kondo, T. Takeuchi, H. Ikuta, Y. Wang, and E. W. Hudson, Nat. Phys. **4**, 696 (2008).

[12] J. Chang, E. Blackburn, A. T. Holmes, N. B. Christensen, J. Larsen, J. Mesot, R. Liang, D. A. Bonn, W. N. Hardy, A. Watenphul, M. Zimmermann, E. M. Forgan, and S. M. Hayden, Nat. Phys. **8**, 871 (2012).

[13] E. Demler, S. Sachdev, and Y. Zhang, Phys. Rev. Lett. **87**, 067202 (2001).

[14] Y. Ohta, T. Tohyama, and S. Maekawa, Phys. Rev. B **43**, 2968 (1991).

[15] E. Pavarini, I. Dasgupta, T. Saha-Dasgupta, O. Jepsen, and O. K. Andersen, Phys. Rev. Lett. **87**, 047003 (2001).

[16] C. Weber, C. Yee, K. Haule, and G. Kotliar, Europhys. Lett. **100**, 37001 (2012).

[17] H. Sakakibara, H. Usui, K. Kuroki, R. Arita, and H. Aoki, Phys. Rev. Lett. **105**, 057003 (2010).

[18] H. Sakakibara, K. Suzuki, H. Usui, S. Miyao, I. Maruyama, K. Kusakabe, R. Arita, H. Aoki, and K. Kuroki, Phys. Rev. B **89**, 224505 (2014).

[19] Y. Y. Peng, G. Dellea, M. Minola, M. Conni, A. Amorese, D. Di Castro, G. M. De Luca, K. Kummer, M. Salluzzo, X. Sun, X. J. Zhou, G. Balestrino, M. Le Tacon, B. Keimer, L. Braicovich, N. B. Brookes, and G. Ghiringhelli, Nat. Phys. **13**, 1201 (2017).

[20] W. Hu, S. Kaiser, D. Nicoletti, C. R. Hunt, I. Gierz, M. C. Hoffmann, M. Le Tacon, T. Loew, B. Keimer, and A. Cavalleri, Nat. Mater. **13**, 705 (2014).

[21] S. Kaiser, C. R. Hunt, D. Nicoletti, W. Hu, I. Gierz, H. Y. Liu, M. Le Tacon, T. Loew, D. Haug, B. Keimer, and A. Cavalleri, Phys. Rev. B **89**, 184516 (2014).

[22] R. Mankowsky, A. Subedi, M. Först, S. O. Mariager, M. Chollet, H. T. Lemke, J. S. Robinson, J. M. Glownia, M. P. Minitti, A. Frano, M. Fechner, N. A. Spaldin, T. Loew, B. Keimer, A. Georges, and A. Cavalleri, Nature (London) **516**, 71 (2014).

[23] G. Kresse and J. Furthmüller, Phys. Rev. B **54**, 11169 (1996).

[24] A. Togo and I. Tanaka, Scr. Mater. **108**, 1 (2015).

[25] I. S. Elfimov, G. A. Sawatzky, and A. Damascelli, Phys. Rev. B **77**, 060504(R) (2008).

[26] J. M. Tranquada, D. E. Cox, W. Kunnmann, H. Moudden, G. Shirane, M. Suenaga, P. Zolliker, D. Vaknin, S. K. Sinha, M. S. Alvarez, A. J. Jacobson, and D. C. Johnston, Phys. Rev. Lett. **60**, 156 (1988).

[27] See Supplemental Material at http://link.aps.org/supplemental/10.1103/PhysRevLett.121.157001 for detailed computational method, summary of $T_{c,\max}$ and d_A of each material, relation between forces and phonon frequency and $T_{c,\max}$, Bader charge analysis of the apical oxygen, charge density difference, phonon and phonon interaction, polaron formation, and DOS with and without polaron, which includes Refs. [28–60].

[28] S. P. Ong, Y. Mo, and G. Ceder, Phys. Rev. B **85**, 081105(R) (2012).

[29] J. B. Torrance, A. Bezinge, A. I. Nazzal, T. C. Huang, S. S. P. Parkin, D. T. Keane, S. J. LaPlaca, P. M. Horn, and G. A. Held, Phys. Rev. B **40**, 8872 (1989).

[30] R. J. Cava, A. Santoro, D. W. Johnson, and W. W. Rhodes, Phys. Rev. B **35**, 6716 (1987).

[31] R. J. Cava, A. Santoro, J. J. Krajewski, R. M. Fleming, J. V. Waszczak, W. F. Peck, and P. Marsh, Physica (Amsterdam) **172C**, 138 (1990).

[32] A. Fuertes, X. Obradors, J. M. Navarro, P. Gomez-Romero, N. Casañ-Pastor, F. Pérez, J. Fontcuberta, C. Miravitlles, J. Rodriguez-Carvajal, and B. Martínez, Physica (Amsterdam) **170C**, 153 (1990).

[33] H. W. Zandbergen, W. T. Fu, J. M. van Ruitenbeek, L. J. de Jongh, G. van Tendeloo, and S. Amelinckx, Physica (Amsterdam) **159C**, 81 (1989).

[34] M. A. Subramanian, J. Gopalakrishnan, C. C. Torardi, P. L. Gai, E. D. Boyes, T. R. Askew, R. B. Flippen, W. E. Farneth, and A. W. Sleight, Physica (Amsterdam) **157C**, 124 (1989).

[35] J. D. Jorgensen, B. W. Veal, A. P. Paulikas, L. J. Nowicki, G. W. Crabtree, H. Claus, and W. K. Kwok, Phys. Rev. B **41**, 1863 (1990).

[36] J. Grybos, D. Hohlwein, T. Zeiske, R. Sonntag, F. Kubanek, K. Eichhorn, and T. Wolf, Physica (Amsterdam) **220C**, 138 (1994).

[37] T. B. Lindemer, B. C. Chakoumakos, E. D. Specht, R. K. Williams, and Y. J. Chen, Physica (Amsterdam) **231C**, 80 (1994).

[38] M. Guillaume, P. Allenspach, W. Henggeler, J. Mesot, B. Roessli, U. Staub, P. Fischer, A. Furrer, and V. Trounov, J. Phys. Condens. Matter **6**, 7963 (1994).

[39] B. W. Veal, A. P. Paulikas, J. W. Downey, H. Claus, K. Vandervoort, G. Tomlins, H. Shi, M. Jensen, and L. Morss, Physica (Amsterdam) **162C–164C**, 97 (1989).

[40] W. Schnelle, E. Braun, H. Broicher, R. Dömel, S. Ruppel, W. Braunisch, J. Harnischmacher, and D. Wohlleben, Physica (Amsterdam) **168C**, 465 (1990).

[41] C. C. Torardi, M. A. Subramanian, J. C. Calabrese, J. Gopalakrishnan, E. M. McCarron, K. J. Morrissey, T. R. Askew, R. B. Flippen, U. Chowdhry, and A. W. Sleight, Phys. Rev. B **38**, 225 (1988).

[42] S. Miura, T. Yoshitake, N. Shohata, and T. Satoh, Physica (Amsterdam) **165C,** 241 (1990).

[43] M. Hervieu, C. Michel, B. Domenges, Y. Laligant, A. Lebail, G. Ferey, and B. Raveau, Mod. Phys. Lett. B **02,** 491 (1988).

[44] T. Watanabe, T. Fujii, and A. Matsuda, J. Phys. Soc. Jpn. **72,** 2924 (2003).

[45] Y. Shimakawa, Y. Kubo, T. Manako, and H. Igarashi, Phys. Rev. B **40,** 11400(R) (1989).

[46] M. A. Subramanian, J. C. Calabrese, C. C. Torardi, J. Gopalakrishnan, T. R. Askew, R. B. Flippen, K. J. Morrissey, U. Chowdhry, and A. W. Sleight, Nature (London) **332,** 420 (1988).

[47] S. S. P. Parkin, V. Y. Lee, E. M. Engler, A. I. Nazzal, T. C. Huang, G. Gorman, R. Savoy, and R. Beyers, Phys. Rev. Lett. **60,** 2539 (1988).

[48] D. E. Cox, C. C. Torardi, M. A. Subramanian, J. Gopalakrishnan, and A. W. Sleight, Phys. Rev. B **38,** 6624 (1988).

[49] S. N. Putilin, E. V. Antipov, O. Chmaissem, and M. Marezio, Nature (London) **362,** 226 (1993).

[50] S. M. Loureiro, E. V. Antipov, J. L. Tholence, J. J. Capponi, O. Chmaissem, Q. Huang, and M. Marezio, Physica (Amsterdam) **217C,** 253 (1993).

[51] B. A. Hunter, J. D. Jorgensen, J. L. Wagner, P. G. Radaelli, D. G. Hinks, H. Shaked, R. L. Hitterman, and R. B. Von Dreele, Physica (Amsterdam) **221C,** 1 (1994).

[52] D. N. Argyriou, J. D. Jorgensen, R. L. Hitterman, Z. Hiroi, N. Kobayashi, and M. Takano, Phys. Rev. B **51,** 8434 (1995).

[53] B. Grande and H. Müller-Buschbaum, Z. Anorg. Allg. Chem. **429,** 88 (1977).

[54] Q. Q. Liu, C. Q. Jin, Y. Yu, F. Y. Li, Z. X. Liu, and R. C. Yu, Int. J. Mod. Phys. B **19,** 331 (2005).

[55] B. Grande and H. Müller-Buschbaum, Z. Anorg. Allg. Chem. **417,** 68 (1975).

[56] X. J. Zhou *et al.*, Phys. Rev. Lett. **95,** 117001 (2005).

[57] A. Subedi, A. Cavalleri, and A. Georges, Phys. Rev. B **89,** 220301(R) (2014).

[58] V. I. Anisimov, M. A. Korotin, J. Zaanen, and O. K. Andersen, Phys. Rev. Lett. **68,** 345 (1992).

[59] Y. Kumagai, F. Oba, I. Yamada, M. Azuma, and I. Tanaka, Phys. Rev. B **80,** 085120 (2009).

[60] C. H. Patterson, Phys. Rev. B **77,** 094523 (2008).

[61] G. Burns and F. H. Dacol, Phys. Rev. B **41,** 4747 (1990).

[62] K. F. McCarty, J. Z. Liu, R. N. Shelton, and H. B. Radousky, Phys. Rev. B **41,** 8792 (1990).

[63] M. Fechner and N. A. Spaldin, Phys. Rev. B **94,** 134307 (2016).

[64] C.-Z. Wang, R. Yu, and H. Krakauer, Phys. Rev. B **59,** 9278 (1999).

[65] I.-S. Yang, H.-G. Lee, N. H. Hur, and J. Yu, Phys. Rev. B **52,** 15078 (1995).

[66] Y. T. Ren, H. Chang, Q. Xiong, Y. Q. Wang, Y. Y. Sun, R. L. Meng, Y. Y. Xue, and C. W. Chu, Physica (Amsterdam) **217C,** 273 (1993).

[67] H. Eisaki, N. Kaneko, D. L. Feng, A. Damascelli, P. K. Mang, K. M. Shen, Z.-X. Shen, and M. Greven, Phys. Rev. B **69,** 064512 (2004).

[68] J. R. Schrieffer and J. S. Brooks, *Handbook of High-Temperature Superconductivity* (Springer, New York, 2007), Chap. 3.4